

Detection of a Large Antigen through the Masking and Exposure of Fragment of Split Luciferase

Cheng Qian,^a Ayumu Ninomiya,^a Natsuki Shibukawa,^a Hiroshi Ueda,^{b,1} Takanobu
Yasuda,^b Bo Zhu^b and Tetsuya Kitaguchi^{b,*}

^a Graduate School of Life Science and Technology, Institute of Science Tokyo, Yokohama, Japan

^b Laboratory for Chemistry and Life Science, Institute of Integrated Research, Institute of Science
Tokyo, Yokohama, Japan

¹ Deceased

*** Corresponding author:**

Tetsuya Kitaguchi, Ph. D.

Laboratory for Chemistry and Life Science, Institute of Integrated Research, Institute of Science
Tokyo, 4259 Nagatsuta-cho, Midori-ku, Yokohama, 226-8501, Japan

E-mail address: kitaguc.t.aa@m.titech.ac.jp

Keywords: protein M, split luciferase, NanoLuc, homogeneous immunoassay

Abstract

We developed PMBiT, an antibody-binding Protein M (PM)-based bioluminescent probe, which detects large antigens through luciferase reconstitution by exposing the luciferase fragment. The detection is achieved by exploiting the principle that the antibody, the large antigen, and PM are not able to form a complex at the same time. The PMBiT is prepared by conjugating PM with HiBiT-based peptide from the split NanoLuc luciferase through click reaction. It retained its binding activity to antibody, and showed bioluminescence upon reconstitution of the luciferase, by assembling with LgBiT, the other fragment of split NanoLuc. Mixing PMBiT with various IgG antibodies resulted in decreased bioluminescence. In contrast, when PMBiT was mixed with IgG bound to its large antigen, such as human C-reactive protein, the decreased bioluminescence was lessened, leading to bioluminescence increase in a dose dependent manner. Molecular dynamics simulations of PM showed that two regions in the C-terminus contribute to steric clashes with antigens due to their relatively rigid structures. Furthermore, *in silico* analysis of the structure suggested that antigen size is the primary factor blocking PMBiT binding to IgG for antigen detection. The immunoassay utilizing PMBiT does not require genetic manipulation of antibodies, allowing for seamless and scalable antibody replacement, and will advance the future of on-site detection and rapid diagnostics.

1. Introduction

Immunoassay utilizing the binding reaction between antibody and antigen, is categorized to two operation principles: heterogeneous and homogeneous immunoassay. Heterogeneous immunoassay such as enzyme-linked immunosorbent assay (ELISA) requires the segregation of antigen-bound antibodies and unbound antibodies for detection of antigens.¹ Despite its high sensitivity and specificity, this immunoassay is usually complex, time-consuming, and laborious, therefore, are not well suited for on-site detection. On the contrary, homogeneous immunoassay does not require repetitive washing steps, thereby simplifies the procedure and is expected to play a significant role in point-of-care testing (POCT), at-home detection, and in field study.²

One prime example of immunosensor in homogeneous immunoassay is known as Quenchbody (Q-body). The working principle of this immunosensor is that the fluorescent dye is quenched by tryptophan residues in the vicinity of antigen-binding pocket and is subsequently released upon the antigen binding.^{3,4} Various types of homogeneous fluorescent immunoassays using the same working principle have been developed, including immunoassay using the PM Q-probe.⁵⁻⁷ The PM Q-probe was generated by conjugating fluorescent dye with Protein M (PM), an antibody-binding protein from the bacteria, *Mycoplasma genitalium*, and enables the conversion of various antibodies into homogeneous immunosensors without genetic manipulation of individual antibody.⁸ However, due to the unique structure of the C-terminal in PM, PM often blocks the binding between antigen and antibody, making biosensor based on PM Q-probe unsuitable for the detection of large molecules. On the other hand, fluorescent immunoassays generally require excitation light, which has limited simple detection on-site.

In this study, we successfully developed a PM-based probe named PMBiT for homogeneous bioluminescence detection of a large antigen through the reconstitution of the split NanoLuc luciferase fragments, HiBiT and LgBiT.⁹⁻¹¹ In the absence of the antigen, PMBiT binds

to the antibody. Since HiBiT conjugated with PM is thought to be sterically embedded within the antibody, the HiBiT fragment remains unapproachable even after the addition of LgBiT (Fig. 1A). In contrast, the binding of the PMBiT to antibody is blocked upon the binding of the large antigen, which leads to the reconstitution of the luciferase, resulting in an increase in bioluminescence (Fig. 1B). Since PMBiT has the capability to achieve homogeneous detection by bioluminescence with simple procedures against various antigens simply by replacing antibodies, this versatility is expected to position PMBiT as a valuable tool across wide range of fields such as scientific research, clinical testing, environmental survey, and food analysis.

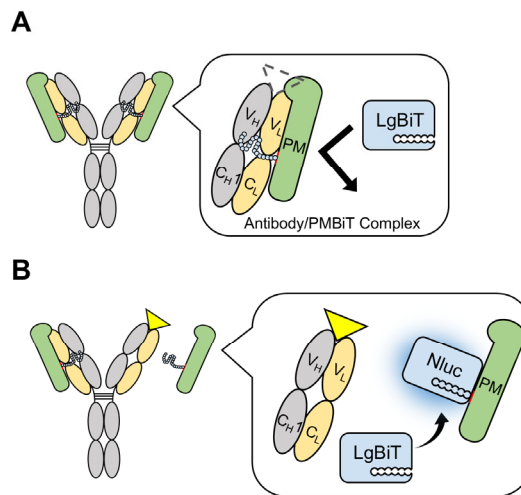


Fig. 1. Concept of the antibody/PMBiT complex-based immunoassay. (A) In the absence of antigen, LgBiT does not access to HiBiT on PMBiT, showing no bioluminescence. (B) In the presence of antigen, LgBiT assembles with HiBiT on PMBiT, leading to the reconstitution of NanoLuc and emission of bioluminescence.

2. Experimental

2.1. Reagents and materials

In this study, the *Escherichia coli* strain XL-10 Gold and BL21(DE3) were purchased from Agilent (CA, USA). SHuffle T7 Express lysY and restriction enzymes were purchased from New England Biolabs (MA, USA). The ligation mix and TALON metal affinity resin were purchased from

Takara bio (Shiga, Japan). while Strep-Tactin Sepharose resin was purchased from IBA Lifesciences (Göttingen, Germany). Human C-Reactive Protein and mouse anti-human C-Reactive Protein monoclonal antibody (MCA5880G) were purchased from Bio-Rad Laboratories (CA, USA). Goat anti-bovine lactoferrin polyclonal antibody (A10-126A) and sheep anti-bovine albumin polyclonal antibody (A10-113A) were purchased from Bethyl Laboratories (TX, USA). ImmunoBlock was purchased from KAC (Kyoto, Japan). 3,3',5,5'-Tetramethylbenzidine (TMBz) was purchased from DOJINDO (Kumamoto, Japan). HRP-conjugated rabbit anti-sheep IgG antibody, HRP-conjugated rabbit anti-goat IgG antibody, and HRP-conjugated goat anti-mouse IgG antibody were purchased from Santa Cruz Biotechnology (TX, USA), Proteintech (IL, USA), and Biosource (CA, USA), respectively. The Gene of NanoLuc was synthesized by Azenta Life Sciences (MA, USA). Other reagents and materials including Bovine serum albumin, Lactoferrin from bovine milk, Coelenterazine h, normal human IgG (143-09501) were purchased from FUJIFILM Wako Pure Chemicals (Osaka, Japan).

2.2. Construction of thermostable PM mutant

The plasmid pET-TrxA2ST-PM-C-(G₃S)₂-His was constructed from our previous research.⁶ The hydrophobicity and percent solvent accessibility of each amino acid in PM was calculated using Discovery Studio. Five hydrophobic amino acids with high solvent accessibility were selected for mutation (Fig. S1A, B). Mutants with either single or multiple mutations were evaluated for thermostability using ELISA. After incubating the PM mutants at 42 °C for both 3 and 6 hours and subsequently adding them to fixed human polyclonal IgGs, the PM3mut (L116S, F222Y, F237S) showed the highest binding activity (Fig. S1C, D). The PM3mut was constructed by overlapping PCR using eight primers (Table S1). The PM insert and the vector were both digested by restriction enzymes XbaI and XhoI. Subsequently, the PM insert was inserted back into the vector through

ligation. Lysine residue at 319th position was afterward mutated to amber codon using the same method (Table S1).

2.3. Production and purification of PM (319 Azide) and LgBiT

pET-TrxA2ST-PM3mut (319 Azide)-C-(G₃S)₂-His, referred to as PM (319 Azide), along with the pEvol-pAzFRS.2.t1 plasmids (a gift from Farren Isaacs, Addgene plasmid #73546) were initially transformed together into BL21(DE3) cells through heat shock (42 °C for 45 seconds, then placed on ice for 3 minutes) and plated onto a LBA plate (Luria broth with 100 µg/mL ampicillin).¹² After overnight incubation at 30 °C, one colony was inoculated into LBA medium containing 100 µg/mL of chloramphenicol and was incubated overnight at 30 °C, 200 rpm for small-scale cultivation. After inoculating the small-scale cultivation to LBA (+chloramphenicol) for large-scale cultivation, the cells were incubated under the same conditions until the OD₆₀₀ reached 0.6. Subsequently, 0.4 mM of IPTG, 0.2% of arabinose, 1 mM of 4-Azido-L-phenylalanine were added, followed by another overnight incubation at 16 °C, 200 rpm. The cells were centrifuged at 5000 g for 10 minutes at 4 °C. The pellet was resuspended using 20 mM phosphate buffer (+NaCl) (20 mM Na₂HPO₄, 20 mM NaH₂PO₄, 500 mM NaCl). Followed by high-pressure cell disruption using Constant Systems Cell Disruptor from Constant Systems (Northants, UK), the lysate supernatant was recovered after centrifugation at 8000g for 10 minutes at 4 °C, mixed with equilibrated TALON metal affinity resin, and rotated for 1 hour at 4 °C. The resin-bound protein was packed into the TALON disposable gravity column and washed 2 times using washing buffer (20 mM phosphate buffer (+NaCl), 20 mM Imidazole). Subsequently, after incubated with elution buffer (20 mM phosphate buffer (+NaCl), 500 mM Imidazole) for 5 minutes, purified PM (319 Azide) was collected without buffer exchange. LgBiT was produced using SHuffle T7 express lysY cells in LBA medium, following the same production and purification steps as PM (319 Azide) without the addition of arabinose or 4-Azido-L-phenylalanine.

2.4. Preparation of HiBiT-DBCO and click reaction

To prepare HiBiT-DBCO, 0.144 mM of HiBiT-based peptide (WKDSGGGSVSGYRLFKKISC), 0.801 mM of TCEP, and 0.32 mM of DBCO-maleimide were mixed in PBST and incubated at room temperature overnight. The product was then isolated and purified through preparative HPLC using Hitachi Chromaster 5430 Diode Array Detector with 5110 pump and 5310 column oven (Tokyo, Japan). The presence of HiBiT-DBCO (calculated m/z: 2601.25) was later confirmed using MALDI-TOF-MS (Fig. S3A). PMBiT was prepared through click reaction using 3 μ M of PM (319 Azide) and 15 μ M of HiBiT-DBCO.¹³ The mixture was incubated in PBS at 37 °C for 30 minutes. The product was then purified using Strep-Tactin Sepharose resin by following the protocol from the manufacturer.

2.5. Enzyme-linked immunosorbent assay

When checking the thermostability of PM mutants, 1 ng/ μ L of the human IgG was immobilized on a transparent high binding 96-well microplate from Corning (Costar 3590) overnight at 4 °C and later washed three times with PBST. 20% ImmunoBlock was then added into each well and incubated for 1 hour at room temperature. After washing three times, 1 ng/ μ L of PM and its mutants were added and incubated for 1 hour at room temperature. Following another triplicate washing, 1/3000 diluted HRP-conjugated StrepTactin was added and incubated for 1 hour. After the washing, 100 μ L of substrate solution containing 0.2 mg/mL TMBz, and 30 mM H₂O₂ in 100 mM of sodium acetate buffer was added into each well. Fifty microliters of 10% (v/v) sulfuric acid was added to stop the reaction after 5 min. Absorbance was measured at 450 nm with 650 nm as the reference wavelength using SH-1000Lab microplate reader from Corona Electric (Ibaraki, Japan).

When checking the binding of PMBiT to the human IgG, 1 ng/ μ L of the human IgG was immobilized on a transparent medium binding 96-well plate from Greiner Bio-One (Item No.:

655001) overnight at 4 °C and later washed three times with PBST. 20% ImmunoBlock was then added into each well and incubated for 1 hour at room temperature. After the same blocking and washing procedure, 0.5 ng/μL of PM, PM (319 Azide), PMBiT were added and incubated for 1 hour at room temperature. Similar steps were taken for the addition of HRP-conjugated StrepTactin, TMBz reaction, and absorbance measurement as mentioned earlier. A substrate solution containing 3 mM H₂O₂ was used for this experiment.

When checking the binding of the antibody to antigen with and without PM, a similar ELISA procedure was used. Briefly, antigens including BSA, bLactoferrin, and hCRP at 10 μg/mL were firstly immobilized on the transparent plate for 16 hours at 4 °C. After washing and blocking, preincubated mixture containing 20 nM of PM and 10 nM of respective antibody was added into the designated well and incubated for 45 minutes. The wells were washed again, and the HRP-conjugated antibodies were added into the respective wells and incubated for 1 hour. The same procedure and solution were used for TMBz reaction and measurement as described earlier.

2.6. Bioluminescence measurement using PMBiT

The respective antibodies (25 nM anti-BSA antibody, 25 nM anti-bLactoferrin antibody, 50 nM anti-hCRP antibody) were initially mixed with the antigens (50 nM BSA, 25 nM bLactoferrin, 90 nM hCRP, or PBST) in PBST, and the 165.5 μL of mixture were incubated at room temperature for 30 minutes. Subsequently, 1 nM of PMBiT was added into the mixtures, resulting in a total volume of 170 μL. The mixtures were incubated again at room temperature for 15 minutes. A premixed substrate solution (50 μL, 1 nM LgBiT, 5 μg/mL Coelenterazine h) was prepared and applied to the 96-well plate in advance. After the incubation, 50 μL of the PMBiT mixtures were added to the wells. After around one minute of reaction time, triplicate measurements were taken using the AB-2350 Phelios luminometer with the following settings: standard measurement mode, 0.1 seconds gate time, 5 seconds measurement time, no filter, 350-670 nm. Controls including

mixture with only LgBiT, mixture with PM and LgBiT, mixture with PMBiT and LgBiT were prepared and measured in the same condition.

For hCRP dose-dependency measurements, two triplicate measurements were taken in different dates with various concentrations of hCRP (0, 0.3, 1, 3, 10, 30, 100 nM). When analyzing the data, the averages of both measurements were used. The dose-response curve was fitted following a four-parameter logistic equation (Eq. 1) using SciDAVis software (version 2.7) with parameter “a” fixed to 1. The limit of detection (LOD) was calculated as the concentration corresponding to the mean of the blank plus three times the standard deviation.

$$y = d + \frac{a-d}{1+(\frac{x}{c})^b} \quad (\text{Equation 1})$$

2.7. Superimposing protein structures

A hundred antigen-bound Fab structures were selected from the RCSB PDB database, starting from the top of the default order (relevancy scoring) in the search results for “Fab complex”. Polymers and complexes containing the same antigen were excluded for efficiency and variety. Among them, the last ten complexes were chosen specifically to balance antigen size by including large antigens. The PDB files of the selected complexes were imported into ChimeraX (version 1.7.1).¹⁴⁻¹⁶ The “MatchMaker” command was used for alignment between PM-bound Fab⁸ (PDB: 4NZR) and each of the selected antigen-bound Fab. Subsequently, the structure of PGT135 Fab from the PM-bound Fab was removed, leaving only the PM and the selected antigen-bound Fab. To identify clashes specifically between PM and each antigen, the “clashes” command was employed to find steric clash where the overlap of pairs of atoms is equal or larger than 0.75 Å. The overlap is calculated by subtracting the distance between the centers of two atoms from the sum of their vdW radii.¹⁷ The allowance for hydrogen bond were also subtracted when a hydrogen

bond is presented between atoms. The clashes were visually represented as orange dots by using the default setting. The log was exported as a text file, and analyzed using Microsoft Excel.

2.8. Molecular dynamics simulation

The PM structure was extracted from the PDB file of PM-bound PGT135 Fab (PDB: 4NZR) by removing the Fab region. Molecular dynamics (MD) simulation was performed using GROMACS (version 2023.2) following the procedure from our previous study.¹⁸⁻²⁰ The AMBER99SB force field was used and the water model was set to SPC/E by default. Energy minimization was performed using the steep algorithm. Both *NVT* and *NPT* equilibrations were performed for 50 ps with the lincs algorithm. MD simulation proceeded for 20 ns with triplicate runs, using random seeds for each run. The root mean square fluctuation (RMSF) were calculated using GROMACS, and the results were visualized using Microsoft Excel. The whole process was performed three times, and the average was obtained and used.

3. Results and Discussion

3.1. Fabrication of PMBiT

To prepare the PMBiT, we substituted the codon of lysine at 319 position of PM3mut (468 aa), which is a thermostable PM generated by introduction of 3 mutations in the hydrophobic amino acids on the surface (Fig. S1), with an amber codon TAG (Fig. S2). Subsequently, *E. coli* BL21 (DE3) cells were transformed with both the PM (319 Azide) and pEvol-pAZ.FRS.2.t1 plasmid DNA, which carries orthogonal tRNA (CUA) and aminoacyl-tRNA synthetase (aaRS) for the site-specific incorporation of unnatural amino acids (Fig. 2A). The residue at position 319 was selected based on the assumption that once conjugated, HiBiT is sterically embedded into the space between PM and antibody (Fig. S1A). After expression and purification of PM (319 Azide), which incorporated 4-azido-L-phenylalanine at the amber codon site, HiBiT-DBCO (Fig. S3A) was

conjugated by click reaction. The SDS-PAGE showed a major band larger than 66 kDa corresponding to PM (319 Azide) after application of HiBiT-DBCO (Fig. S3B), suggesting the formation of PMBiT through the conjugation of HiBiT-DBCO.

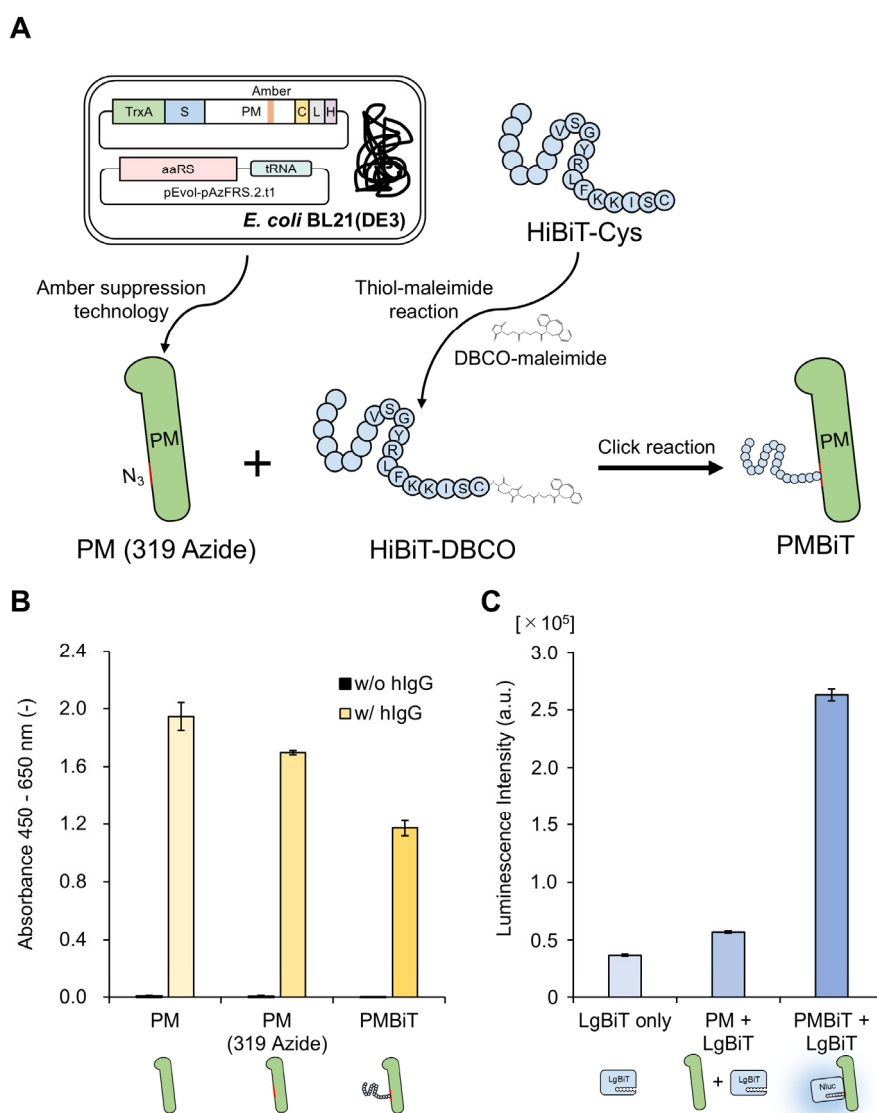


Fig. 2. Design, preparation, and characterization of the PMBiT probe. (A) Design and the preparation of PMBiT. TrxA: thioredoxin, S: twin-strep-tag, C: cys-tag, L: (G₃S)₂ linker, H: His-tag. (B) Binding activity of PM, PM (319 Azide), PMBiT against human polyclonal IgGs by ELISA. (C) Reconstitution of the luciferase confirmed by bioluminescence. All data are shown as means ± standard deviation (n = 3)

When the binding of PMBiT to the human antibody was examined by ELISA (Fig. 2B), we found that both PM (319 Azide) and PMBiT showed weaker absorbance signals than the unmodified PM. The modification on PM led to a decreased affinity of PMBiT to the antibody, which would be a favorable for this detection system using PMBiT. The lower affinity of PMBiT aligns with the working principle that PMBiT does not bind to the antibody once antigen binds to the antibody. We next investigated whether the luciferase reconstitution leads to bioluminescence emission (Fig. 2C). The bioluminescence from the reconstituted NanoLuc was much higher than the signal from the LgBiT, both with and without the PM, suggesting that the generation of PMBiT, setting the stage for the following experiments.

3.2. Bioluminescence response by masking and exposure of HiBiT

To examine whether an antibody masks HiBiT on PMBiT, we measured the bioluminescence intensity of PMBiT with and without antibodies such as anti-bovine serum albumin (BSA) sheep IgG, anti-bovine lactoferrin (bLactoferrin) goat IgG, or anti-human C-reactive protein (hCRP) mouse IgG. For all three antibody/PMBiT mixtures, we found the decreased bioluminescence intensity with IgGs, suggesting that HiBiT on PMBiT is sterically embedded by binding of antibody (Fig. 3A-C). Although anti-BSA IgG induced a slightly greater decrease in bioluminescence intensity than anti-bLactoferrin or anti-hCRP IgGs, the variation would be owing to the different affinities between PMBiT and antibodies of distinct species, such as sheep, goat, or mouse.⁸ Upon mixing the respective antigen of each antibody followed by PMBiT, the bioluminescence intensity was comparable with BSA (67 kDa), but showed increased bioluminescence intensity with bLactoferrin (80 kDa) and hCRP (120 kDa) (Fig. 3C). For the further evaluation of PMBiT in the detection of hCRP (120 kDa) which showed the largest bioluminescence response, we confirmed that increased bioluminescence intensity was in a dose-

dependent manner, with an EC_{50} value of 2.0 nM and a limit of detection (LOD) of 0.66 nM. (Fig. 3D).

To examine whether the bioluminescence response was due to PMBiT no longer binding to the antibody as the result of the antibody binding to the antigen, we performed an ELISA to check the binding of the antibody to antigen with and without PM (Fig. 3E). The addition of PM did not significantly affect the absorbance for BSA as antigen, while it slightly decreased the absorbance for bLactoferrin and substantially for hCRP (Fig. 3F), suggesting the binding of antigens like bLactoferrin and hCRP to the antibody is blocked by PM. Since the absorbance of the antibody/PM complex becomes weaker against these larger protein antigens, it is reasonable to assume that the antibody cannot bind to both the large antigen and PM simultaneously. This assumption also explains why PMBiT is blocked from binding to IgG by the steric hindrance of large antigens.

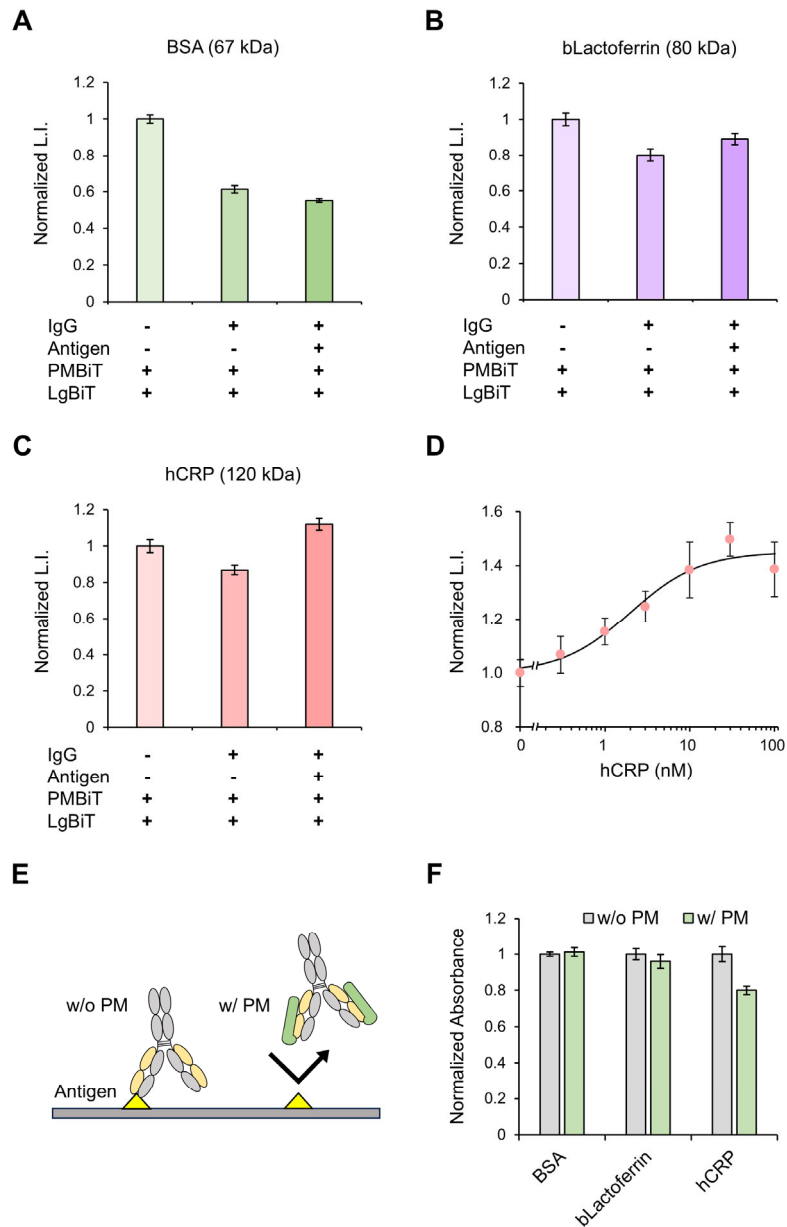


Fig. 3. Bioluminescence response and binding activity of antibody/PMBiT complexes. (A) Bioluminescence response of BSA antibody/PMBiT complex against BSA (67 kDa). (B) bLactoferrin antibody/PMBiT complex against bLactoferrin (80 kDa). (C) hCRP antibody/PMBiT complex against hCRP (120 kDa). (D) Dose-response relationship for hCRP antibody/PMBiT complex against hCRP. All data are shown as means \pm standard deviation ($n = 3$) (E) Concept of the binding of the antibody/PM complex against the antigen. (F) Binding activities of antibody/PM complexes against antigens by ELISA.

3.3. Estimation of steric clash between antigens and PM on antibodies

In order to further explore the relationship between PM hindrance and antigen size, 100 antigen-bound Fab structures from PDB with various sizes of antigens were selected and superimposed with PM (PDB: 4NZR) (Table S2). Among the superimposed structures, gHgL of Varicella-zoster virus in complex with Fab (108 kDa) (PDB: 4XHJ) was carefully studied because of the largest number of steric clash with PM (Fig. 4A, B).²¹ Steric clash is visualized as orange dots, representing the overlap of pairs of atoms with distances equal to or greater than 0.75 Å between the antigen and PM. The antigen gHgL exhibited 4316 clashes with PM, especially with the C-terminus of PM (Fig. 4B). For better understanding, the C-terminus of PM was categorized into three regions, which collectively account for over 50% of the clashes: regions 1 (406-420) and 3 (448-468) each containing one alpha helix, and region 2 (424-440) comprising two beta sheets (Fig. 4C). Upon investigating the 100 superimposed complexes, we found strong correlation coefficients, 0.78 – 0.91 between the total number of clashes and the clashes on regions 1, 2, and 3 in the C-terminus of PM (Fig. 4D). These results are consistent with the finding that PM blocks antigen-antibody binding, as reported previously⁸, and matches with our expectation that there are many steric clashes between antigen and the C-terminus of PM. Molecular Dynamics (MD) simulations were performed to find out which region primarily causes the clashes. The Root Mean Square Fluctuation (RMSF) analysis for the flexibility of PM showed that the overall fluctuation was low, while region 3 exhibited higher RMSF values compared to regions 1 and 2, suggesting that region 3 has greater flexibility (Fig. 4E). We interpreted that regions 1 and 2 contribute more for blocking PMBiT from binding to large antigen-bound antibodies, resulting in the exposure of HiBiT.

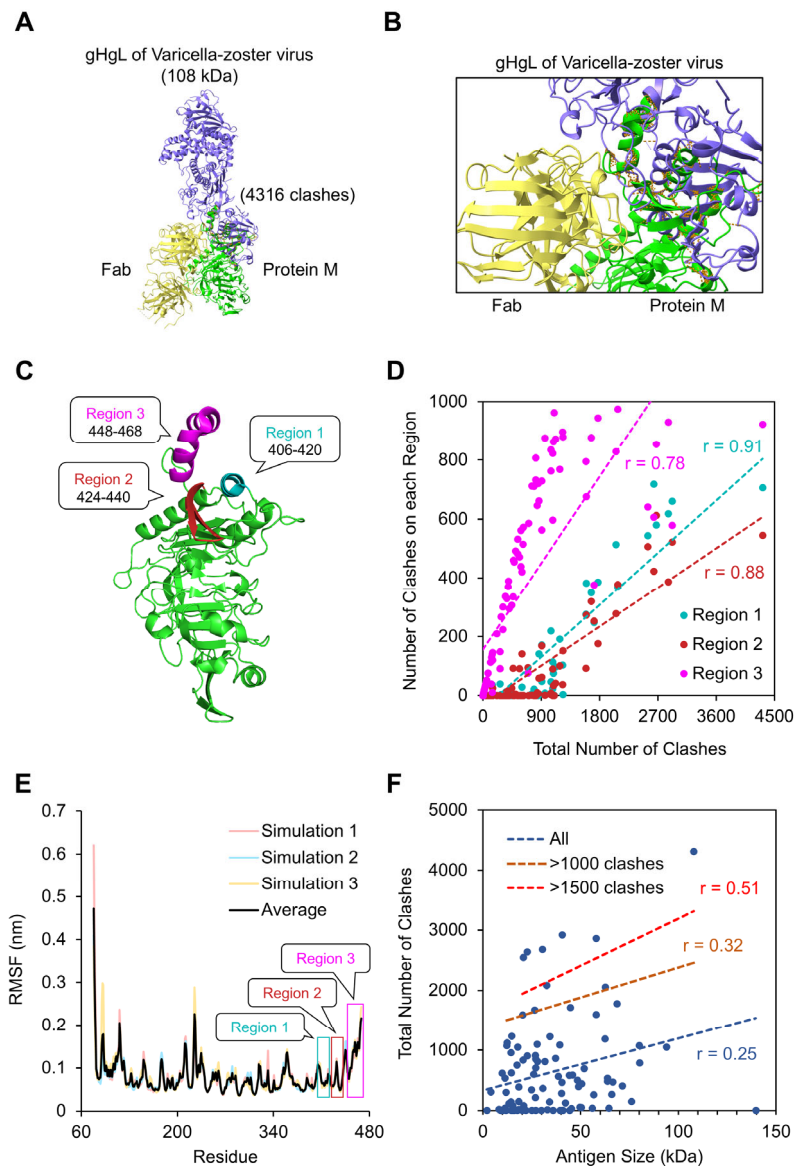


Fig. 4. Examination of the steric relationship between PM and antigen. (A) The superimposition of antigen-bound Fab (PDB: 4XHJ) and PM. (B) A magnified view of the interaction between the Fab and the C-terminus of PM. The orange dots indicate steric clashes, overlapping between two structures. (C) The structure of PM and its three regions near its C-terminus. Region 1 (406 to 420) is indicated in cyan, region 2 (424 to 440) in red, and region 3 (448 to 468) in magenta. (D) Correlation between total number of clashes and the number of clashes on region 1, 2, and 3 for 100 antigen-bound Fab superimposed with PM. (E) The RMSF of the PM. Three simulations were colored in red, blue, and yellow, and the average in black. All data are shown as means \pm standard deviation ($n = 3$) (F) Correlation between antigen size and total number of clashes for 100 antigens-bound Fab superimposed with PM.

When we examined the relationship between steric clashes and antigen sizes, we found a low correlation coefficient, 0.25 between antigen size and the total number of clashes for the 100 superimposed complexes. For complexes with more than 1000 and 1500 clashes, the correlation coefficients were 0.32 and 0.51, respectively, which are higher than those of all other complexes (Fig. 4F). These results suggest that complexes with increased clashes are more likely to be complexed with larger antigens, and that antigen size is the primary factor contributing to the blocking of PMBiT from binding to the antibody. The superimposed structure, size of the antigen, and the number of clashes between PM and the antigen, help in estimating which antigen may be detectable using the PMBiT probe.

4. Conclusions

In this study, we developed PMBiT, a thermostable PM-based probe applicable to large antigen detection by emitting bioluminescence through reconstitution of luciferase. The masking and exposure of conjugated HiBiT peptide in PMBiT were examined by employing various antibodies and respected antigens. This antibody/PMBiT complex-based detection demonstrates its capability in detecting larger antigens by altering the accessibility of HiBiT within PMBiT. Superimposed structures of PM and Fab bound to various antigens revealed that antigen size significantly contributes to the steric clashes between the antigen and PM. The MD simulations showed certain regions within the C-terminus of PM as more rigid, implying their greater role in blocking PMBiT from binding to the antibody during the presence of antigens. This PMBiT probe introduces a new approach by combining PM and split NanoLuc luciferase system to generate a bioluminescence detection system. This study presents a new strategy for utilizing PM in antigen detection, addressing the limitations of the previous PM-based sensors that were restricted to the detection of small antigens, by extending the detection range to include larger antigens.

Data availability

Raw data will be made available from the corresponding author upon reasonable request.

Author contributions

C.Q., A.N., and N.S. performed the experiments. C.Q. and B.Z. performed the *in silico* experiment including superimposition and molecular dynamics simulations. C.Q., T.Y., B.Z., and T. K. wrote and edited the manuscript. T.K. and H.U. conceived this study.

Conflicts of interest

The authors declare the following financial interest, which may be considered a potential competing interest: H.U., T.Y., B.Z., and T.K. received honoraria from HikariQ Health Inc. for an unrelated project.

Acknowledgements

We thank Masaki Takahashi for his valuable experimental help in this study. This work was supported by the Japan Society for the Promotion of Science, Japan (JSPS KAKENHI Grant Numbers JP22H05176 (T.K.), JP24K01264 (T.K.), and JP24H01123 (B.Z.)), the Japan Science and Technology Agency, Japan (JST SPRING Grant Number JPMJSP2106 (C.Q.)), Grant-in-Aid for Pioneering Research from Organization for Fundamental Research of Institute of Innovative Research, Tokyo Institute of Technology (B.Z.), and a research grant from the Nakatani Foundation (H.U. and T.K.).

References

1. E. Engvall and P. Perlmann, *J Immunol*, 1972, **109**, 129-135.
2. I. A. Darwish, *Int J Biomed Sci*, 2006, **2**, 217-235.
3. J. H. Dong and H. Ueda, *Sensors-Basel*, 2021, **21**, 1223.

4. R. Abe, H. Ohashi, I. Iijima, M. Ihara, H. Takagi, T. Hoshika and H. Ueda, *J Am Chem Soc*, 2011, **133**, 17386-17394.
5. A. Inoue, Y. Ohmuro-Matsuyama, T. Kitaguchi and H. Ueda, *Acs Sensors*, 2020, **5**, 3457-3464.
6. J. H. Dong, C. Miyake, T. Yasuda, H. Oyama, I. Morita, T. Tsukahara, M. Takahashi, H. J. Jeong, T. Kitaguchi, N. Kobayashi and H. Ueda, *Biosens Bioelectron*, 2020, **165**, 112425.
7. T. Yasuda, A. Inoue, T. Kitaguchi and H. Ueda, *Chem Commun*, 2021, **57**, 8206-8209.
8. R. K. Grover, X. Y. Zhu, T. Nieuwma, T. Jones, I. Boero, A. S. MacLeod, A. Mark, S. Niessen, H. J. Kim, L. Kong, N. Assad-Garcia, K. Kwon, M. Chesi, V. V. Smider, D. R. Salomon, D. F. Jelinek, R. A. Kyle, R. B. Pyles, J. I. Glass, A. B. Ward, I. A. Wilson and R. A. Lerner, *Science*, 2014, **343**, 656-661.
9. M. P. Hall, J. Unch, B. F. Binkowski, M. P. Valley, B. L. Butler, M. G. Wood, P. Otto, K. Zimmerman, G. Vidugiris, T. Machleidt, M. B. Robers, H. A. Benink, C. T. Eggers, M. R. Slater, P. L. Meisenheimer, D. H. Klaubert, F. Fan, L. P. Encell and K. V. Wood, *Acs Chemical Biology*, 2012, **7**, 1848-1857.
10. A. S. Dixon, M. K. Schwinn, M. P. Hall, K. Zimmerman, P. Otto, T. H. Lubben, B. L. Butler, B. F. Binkowski, T. Machleidt, T. A. Kirkland, M. G. Wood, C. T. Eggers, L. P. Encell and K. V. Wood, *Acs Chemical Biology*, 2016, **11**, 400-408.
11. M. K. Schwinn, T. Machleidt, K. Zimmerman, C. T. Eggers, A. S. Dixon, R. Hurst, M. P. Hall, L. P. Encell, B. F. Binkowski and K. V. Wood, *Acs Chemical Biology*, 2018, **13**, 467-474.
12. M. Amiram, A. D. Haimovich, C. G. Fan, Y. S. Wang, H. R. Aerni, I. Ntai, D. W. Moonan, N. J. Ma, A. J. Rovner, S. H. Hong, N. L. Kelleher, A. L. Goodman, M. C. Jewett, D. Söll, J. Rinehart and F. J. Isaacs, *Nat Biotechnol*, 2015, **33**, 1272-1279.
13. H. C. Kolb, M. G. Finn and K. B. Sharpless, *Angew Chem Int Ed*, 2001, **40**, 2004-2021.

14. T. D. Goddard, C. C. Huang, E. C. Meng, E. F. Pettersen, G. S. Couch, J. H. Morris and T. E. Ferrin, *Protein Sci*, 2018, **27**, 14-25.
15. E. F. Pettersen, T. D. Goddard, C. R. C. Huang, E. E. C. Meng, G. S. Couch, T. I. Croll, J. H. Morris and T. E. Ferrin, *Protein Sci*, 2021, **30**, 70-82.
16. E. C. Meng, T. D. Goddard, E. F. Pettersen, G. S. Couch, Z. J. Pearson, J. H. Morris and T. E. Ferrin, *Protein Sci*, 2023, **32**, e4792.
17. J. Tsai, R. Taylor, C. Chothia and M. Gerstein, *Journal of Molecular Biology*, 1999, **290**, 253-266.
18. M. J. Abraham, T. Murtola, R. Schulz, S. Páll, J. C. Smith, B. Hess and E. J. S. Lindahl, 2015, **1**, 19-25.
19. H. Bekker, H. J. C. Berendsen, E. J. Dijkstra, S. Achterop, R. Vondrumen, D. Vanderspoel, A. Sijbers, H. Keegstra, B. Reitsma and M. K. R. Renardus, *Physics Computing '92*, 1993, 252-256.
20. B. Zhu, C. Qian, H. X. Tang, T. Kitaguchi and H. Ueda, *Biochemistry*, 2023, **62**, 309-317.
21. Y. Xing, S. L. Oliver, T. Nguyen, C. Ciferri, A. Nandi, J. Hickman, C. Giovani, E. Yang, G. Palladino, C. Grose, Y. Uematsu, A. E. Lilja, A. M. Arvin and A. Carfi, *P Natl Acad Sci USA*, 2015, **112**, 6056-6061.